Journal of Solid Mechanics Vol. 8, No. 4 (2016) pp. 859-874

Non-Local Thermo-Elastic Buckling Analysis of Multi-Layer Annular/Circular Nano-Plates Based on First and Third Order Shear Deformation Theories Using DQ Method

Sh. Dastjerdi [1], M. Jabbarzadeh [2, *]

[1] *Department of Mechanical Engineering, Shahrood Branch, Islamic Azad University, Shahrood, Iran*
[2] *Department of Mechanical Engineering, Mashhad Branch, Islamic Azad University, Mashhad, Iran*

Received 1 August 2016; accepted 7 October 2016

ABSTRACT

In present study, thermo-elastic buckling analysis of multi-layer orthotropic annular/circular graphene sheets is investigated based on Eringen's theory. The moderately thick and also thick nano-plates are considered. Using the non-local first and third order shear deformation theories, the governing equations are derived. The van der Waals interaction between the layers is simulated for multi-layer sheets. The stability governing equations are obtained according to the adjacent equilibrium estate method. The constitutive equations are solved by applying the differential quadrature method (DQM). Applying the differential quadrature method, the ordinary differential equations are transformed to algebraic equations. Then, the critical temperature is obtained. Since there is not any research in thermo-elastic buckling analysis of multi-layer graphene sheets, the results are validated with available single layer articles. The effects of non-local parameter, the values of van der Waals interaction between the layers, third to first order shear deformation theory analyses, non-local to local analyses, different values of Winkler and Pasternak elastic foundation and analysis of bi-layer and triple layer sheets are investigated. It is concluded that the critical temperature increases and tends to a constant value along the rise of van der Waals interaction between the layers.

Keywords : Multi-layer orthotropic annular/circular graphene sheets; Non-local first and third order shear deformation theories; Thermo-elastic buckling analysis; Differential quadrature method (DQM).

1 INTRODUCTION

FOR the first time Bohem et al [1] introduced the graphene as a net of carbon atoms which is formed in hexagonal shape frequently and regularly with covalent bonds between the carbon atoms. Many scientists believed that this special shape with thickness of one carbon atom cannot be stable, so the investigations were delayed until Novoselov and Geim [2] are succeeded to produce a stable single layer graphene sheet. The special shape of graphene sheet leads to unusual mechanical, thermal and electrical properties and the high stiffness to

*Corresponding author. Tel.: +985136625046.
E-mail address: jabbarzadeh@mshdiau.ac.ir (M. Jabbarzadeh).

inertia ratio. These significant properties persuade researchers to engage them within other substances. So, analysis of mechanical properties of nanostructures is significant.

Extraordinary mechanical behavior of graphene convinced many researchers to study the mechanical behavior of nano-structures. The stability analysis is one of the challenging and complicated aspects in mechanical engineering. Buckling analysis is one of the stability issues that many researchers tried to predict the critical load for structures. Graphene sheet can be simulated as a classical plate to study its mechanical behavior. However, in nano sizes the interactions between the atoms cannot be neglected and must be considered in calculations. The obtained results from classical theories in elasticity and experimental tasks show that using of the classical elasticity theory leads to significant differences between the results. According to the vast computational expenses of nano-structures analyses when applying atomic lattice dynamics and molecular dynamic simulations, there is a great interest in applying continuum mechanics for analysis of such structures. In recent years, various size dependent continuum theories have been introduced such as couple stress theory [3], strain gradient elasticity theory [4-6], modified couple stress theory [7-10] and non-local elasticity theory [11-13]. These theories are comprised of information about the inter-atomic forces and internal lengths that is introduced as small scale effect in non-local elasticity theory [14]. Through these methods, the Eringen's non-local elasticity theory [12] has been used much more than the others. In this theory, the stress at a reference point is a function of the strain field at every point in the body. An experimental work was presented by Wen et al [15] to examine the buckling mechanism of graphene nanosheets. They found that when the sheets buckled the graphene layers undergo sharp kinking. However, the graphene layers can survive kinking without fracture due to their exceptional flexibility. Ghorbanpour Arani et al [16] applied non-local DQM for large amplitude vibration of annular boron nitride sheets on non-linear elastic medium. They concluded that with increasing non-local parameter, the frequency of the coupled system becomes lower. Mohammadi et al [17] studied the small scale effect on the vibration of orthotropic plates embedded in an elastic medium and under biaxial in-plane pre-load via non-local elasticity theory. Their results show that with the decrease of in-plane pre-loads the curves isotropic and orthotropic non-dimensional frequency approaches close to each other. Dastjerdi et al [18] applied the non-local elasticity theory of Eringen to find the deformation response of a single layer sector embedded in elastic matrix under uniform transverse loading. They found that the maximum deflection reduces with increase of the non-local parameter. Anjomshoa et al [19] investigated Frequency analysis of embedded orthotropic circular and elliptical micro/nano-plates using non-local variational principle. They proved that the natural frequencies depend on the non-locality of the micro/nano-plate, especially at small dimensions. Pradhan [20] investigated the buckling analysis of rectangular graphene sheets based on non-local TSDT elasticity theory. He improved the Navier solution for all simply supported edges and obtained the buckling temperature. His results show that the non-local to local critical temperature is always equal or less than unit and the TSDT analysis gives more accurate results. He et al. [21] described van der Waals interaction between the layers of multi-layered graphene sheets by an explicit formula based on the continuum mechanics and a multiple-elastic beam model. Scarpa et al. [22] studied both circular and rectangular graphene sheets subjected to point loading based on a special equivalent atomistic-continuum model. They found that the rectangular SLGSs show a different distribution of the geometrical and mechanical properties, compared to the circular configuration. Samaei et al [23] studied buckling of graphene sheets based on FSDT non-local elasticity theory. They investigated the small scale effects on buckling load. Zenkour et al [24] considered the thermo-elastic buckling of graphene sheets embedded in Winkler-Pasternak elastic matrix. They used non-linear CPLT. Their results declare that the critical temperature in clamped-free boundary conditions is more than the other boundary conditions. Wang et al [25] developed the non-local theory for thermo-elastic buckling analysis of nano plates considering the linear strain field in absence of elastic foundation. They calculated the critical temperature only for simply supported boundary conditions.

In this paper, the non-linear thermo-elastic buckling of multi-layer graphene sheets embedded in Winkler-Pasternak elastic matrix is investigated based on non-local first and third order shear deformation theories. The governing equations are obtained for multi-layer annular/circular graphene sheets. The critical temperature is calculated for various types of boundary conditions, different values of the van der Waals interactions between the layers and the values of elastic foundation. The effect of non-local parameter is studied on critical temperature.

2 GOVERNING EQUATIONS

2.1 TSDT Formulation

A multi-layer annular/circular graphene sheet with thickness h, inner radius r_i, outer radius r_0, is shown in Fig. 1. The classical plate theory (CLPT) neglects the effects of shear stress through the thickness of the plate. CLPT

usually is being used for thin plates, because, the effect of shear stress through the thickness is inconsiderable. So, the obtained results of CLPT analysis are accurate for thin plates. However, the first order shear deformation theory (FSDT) should be used instead of CLPT for moderately thick plates. The shear stress is considered linear through the thickness and the FSDT requires the shear correction factor. Also in the FSDT shear stress is not satisfied at the top and bottom of the plate. The TSDT can be used to obtain the most accurate results, specially for thick plates. In this theory, the shear correction factor is not required and the shear stress can be satisfied at the top and bottom of the plate. In this paper, it is aimed to obtain the most accurate results, so the first and third order shear deformation theories (FSDT, TSDT) are used to derive the governing equations. As it is mentioned, the TSDT analysis gives the more accurate results in comparison with CLPT (Classical Plate Theory) and FSDT. The TSDT analysis does not have the weaknesses of the other theories by considering the shear stress effects through the thickness of the plate (weakness of the CLPT) and satisfying the boundaries for shear stress at the surfaces of the plate (weakness of FSDT) Whatever the higher theory of the plates is exerted, the number of governing equations increases. Consequently, the computational process will be more complex and time consuming. So, choosing the theory depends on the initial conditions of the issue and the expected accuracy. According to the third-order shear deformation theory, the displacement field can be expressed as follow. The index i represents the layer number, for example $i=l$ refers to the upper layer under transverse load and $i=n$ the bottom layer rested on the elastic foundation ($i=1, 2, 3\ldots n$).

$$Ui(r,z)=ui(r)+z\psi i_1(r)+z^3\psi i_2(r) \tag{1}$$

$$Vi(r,z)=0 \tag{2}$$

$$Wi(r,z)=wi(r) \tag{3}$$

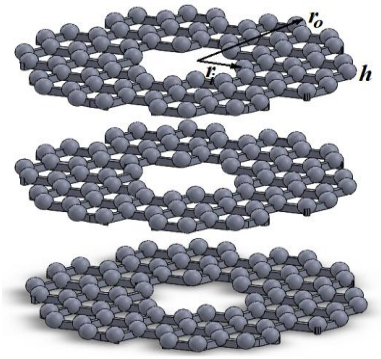

Fig.1
Triple layer annular nano plate.

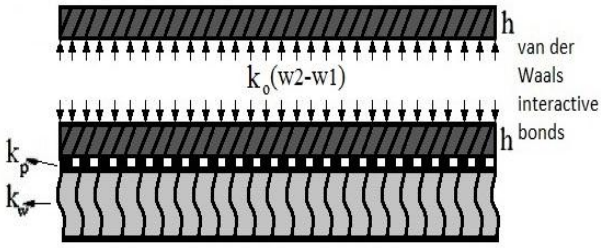

Fig.2
Bi-layer graphene sheet rested on Winkler-Pasternak elastic foundation considering the van der Waals interaction between the layers.

The van der Waals interaction and elastic matrix are pictured in Fig. 2. k_w and k_p are the Winkler and Pasternak stiffness coefficients of elastic foundation respectively. The term $k_0(w_2-w_1)$ refers to the van der Waals interaction bonds between the layers in Fig. 2. and k_0 is the van der Waals stiffness.

In Eqs. (1-3), ui and wi are the displacement components of the mid-plane along the r and z directions, respectively. ψi_1 explains the rotation functions of the transverse normal about circumferential and radial directions. ψi_2 is only a mathematical parameter. Considering the von-Karman assumptions, the strain field are expressed as follows:

$$\varepsilon i_r = \frac{\partial ui}{\partial r} + z\frac{\partial \psi i_1}{\partial r} + z^3\frac{\partial \psi i_2}{\partial r} + \frac{1}{2}\left(\frac{dwi}{dr}\right)^2 \tag{4}$$

$$\varepsilon i_\theta = \frac{ui}{r} + z\frac{\psi i_1}{r} + z^3\frac{\psi i_2}{r} \tag{5}$$

$$\gamma i_{rz} = \frac{dwi}{dr} + \psi i_1 + 3z^2\psi i_2 \tag{6}$$

The effects of atomic forces are significant in nano scales and it must be entered into the fundamental relations as material parameters [12,18]. In non-local theory, the stress at reference point X is a function of strain field in every point on the sheet. Eringen presented a differential form of the non-local relations as follow [12]:

$$\left(1-\mu\nabla^2\right)\sigma^{NL} = \sigma^L = C:\varepsilon, \mu = \left(e_0 a\right)^2$$
$$C = \begin{bmatrix} \frac{E_r}{1-\nu_{r\theta}\nu_{\theta r}} & \frac{\nu_{\theta r}E_\theta}{1-\nu_{r\theta}\nu_{\theta r}} & 0 \\ \frac{\nu_{r\theta}E_\theta}{1-\nu_{r\theta}\nu_{\theta r}} & \frac{E_\theta}{1-\nu_{r\theta}\nu_{\theta r}} & 0 \\ 0 & 0 & G_{rz} \end{bmatrix} \tag{7}$$

In Eq. (7), a is internal characteristic length, and e_0 is material constant which is determined by experiment. The parameter $e_0 a$ is the nan-local parameter exposing the small-scale effect on the nano-size structures. C is the material properties tensor which is considered orthotropic as shown in Eq. (7). The value of the non-local parameter (μ) depends on boundary conditions, chirality, number of walls, and the nature of motions and often is taken between 0 to 2 *nm* [26]. By applying Eq. (7), the non-local stress components can be expressed in cylindrical coordinates system below [12]:

$$\sigma i_r^{NL} - \mu\left(\nabla^2\sigma i_r^{NL} - \frac{2}{r^2}\left(\sigma i_r^{NL} - \sigma i_\theta^{NL}\right)\right) = \sigma i_r^L \tag{8}$$

$$\sigma i_\theta^{NL} - \mu\left(\nabla^2\sigma i_\theta^{NL} + \frac{2}{r^2}\left(\sigma i_r^{NL} - \sigma i_\theta^{NL}\right)\right) = \sigma i_\theta^L \tag{9}$$

$$\sigma i_{rz}^{NL} - \mu\left(\nabla^2\sigma i_{rz}^{NL} - \frac{1}{r^2}\sigma i_{rz}^{NL}\right) = \sigma i_{rz}^L \tag{10}$$

Also, ∇^2 is the Laplacian operator in Cylindrical coordinates system as follow:

$$\nabla^2 = \frac{d^2}{dr^2} + \frac{1}{r}\frac{d}{dr} \tag{11}$$

Considering Eqs. (8-10) into Eq. (7) leads to:

$$\begin{Bmatrix} \sigma i_r^{NL} \\ \sigma i_\theta^{NL} \\ \sigma i_{rz}^{NL} \end{Bmatrix} - \mu \begin{Bmatrix} \nabla^2 \sigma i_r^{NL} - \frac{2}{r^2}\left(\sigma i_r^{NL} - \sigma i_\theta^{NL}\right) \\ \nabla^2 \sigma i_\theta^{NL} + \frac{2}{r^2}\left(\sigma i_r^{NL} - \sigma i_\theta^{NL}\right) \\ \nabla^2 \sigma i_{rz}^{NL} - \frac{1}{r^2}\sigma i_{rz}^{NL} \end{Bmatrix} = \begin{bmatrix} \frac{E_r}{1-\nu_{r\theta}\nu_{\theta r}} & \frac{\nu_{\theta r}E_\theta}{1-\nu_{r\theta}\nu_{\theta r}} & 0 \\ \frac{\nu_{r\theta}E_\theta}{1-\nu_{r\theta}\nu_{\theta r}} & \frac{E_\theta}{1-\nu_{r\theta}\nu_{\theta r}} & 0 \\ 0 & 0 & G_{rz} \end{bmatrix} \begin{Bmatrix} \varepsilon_r \\ \varepsilon_\theta \\ \varepsilon_{rz} \end{Bmatrix} - \begin{bmatrix} \frac{E_r \alpha \cdot \Delta T}{1-\nu_{r\theta}} \\ \frac{E_\theta \alpha \cdot \Delta T}{1-\nu_{\theta r}} \\ 0 \end{bmatrix} \tag{12}$$

$\alpha \cdot \Delta T$ is thermal strain, in which α is thermal diffusivity and ΔT is the temperature difference. The non-local stress resultant components $Ni_j^{NL}, Mi_j^{NL}, Hi_j^{NL} (j = r, \theta)$ and Q_r^{NL}, Y_r^{NL} can be formulated as follows:

$$(Mi_r, Mi_\theta)^{NL} = \int_{-\frac{h}{2}}^{\frac{h}{2}} (\sigma i_r, \sigma i_\theta)^{NL} z dz \tag{13}$$

$$(Ni_r, Ni_\theta, Qi_r)^{NL} = \int_{-\frac{h}{2}}^{\frac{h}{2}} (\sigma i_r, \sigma i_\theta, \sigma i_{rz})^{NL} dz \tag{14}$$

$$Yi_r^{NL} = \int_{-\frac{h}{2}}^{\frac{h}{2}} \sigma i_{rz}^{NL} z^2 dz \tag{15}$$

$$(Hi_r, Hi_\theta)^{NL} = \int_{-\frac{h}{2}}^{\frac{h}{2}} \left(\sigma i_r, \sigma i_\theta\right)^{NL} z^3 dz \tag{16}$$

Substituting Eq. (12) into Eqs. (13-16), the local and non-local force, moment and shear force components can be developed as follows:

$$\left(Ni, Mi, Hi\right)_r^{NL} - \mu\left(\nabla^2\left(Ni, Mi, Hi\right)_r^{NL} - \frac{4}{r^2}\frac{\partial\left(Ni, Mi, Hi\right)_{r\theta}^{NL}}{\partial\theta} - \frac{2}{r^2}\left(\left(\left(Ni, Mi, Hi\right)_r^{NL} - \left(Ni, Mi, Hi\right)_\theta^{NL}\right)\right)\right) = \left(Ni, Mi, Hi\right)_r^{L} \tag{17}$$

$$\left(Ni, Mi, Hi\right)_\theta^{NL} - \mu\left(\nabla^2\left(Ni, Mi, Hi\right)_\theta^{NL} + \frac{4}{r^2}\frac{\partial\left(Ni, Mi, Hi\right)_{r\theta}^{NL}}{\partial\theta} + \frac{2}{r^2}\left(\left(\left(Ni, Mi, Hi\right)_\theta^{NL} - \left(Ni, Mi, Hi\right)_\theta^{NL}\right)\right)\right) = \left(Ni, Mi, Hi\right)_\theta^{L} \tag{18}$$

$$(Qi, Yi)_{rz}^{NL} - \mu\left(\nabla^2 (Qi, Yi)_{rz}^{NL} - \frac{1}{r^2}(Qi, Yi)_{rz}^{NL}\right) = (Qi, Yi)_{rz}^{L} \tag{19}$$

$Ni_j^L, Mi_j^L, Hi_j^L (j = r, \theta)$ and Qi_r^L, Yi_r^L are the local form of stress resultants which are defined for orthotropic material below:

$$Ni_r^L = \frac{E_r h}{1-\nu_{r\theta}\nu_{\theta r}}\left(\frac{dui}{dr} + \frac{1}{2}\left(\frac{dwi}{dr}\right)^2 - \alpha \cdot \Delta T\right) + \frac{\nu_{r\theta}E_\theta h}{1-\nu_{r\theta}\nu_{\theta r}}\left(\frac{ui}{r} - \alpha \cdot \Delta T\right) \tag{20}$$

$$Ni_\theta^L = \frac{\nu_{r\theta}E_\theta h}{1-\nu_{r\theta}\nu_{\theta r}}\left(\frac{dui}{dr} + \frac{1}{2}\left(\frac{dwi}{dr}\right)^2 - \alpha \cdot \Delta T\right) + \frac{E_\theta h}{1-\nu_{r\theta}\nu_{\theta r}}\left(\frac{ui}{r} - \alpha \cdot \Delta T\right) \tag{21}$$

$$Qi_r^L = \frac{1}{4} G_{rz} \psi i_2 h^3 + G_{rz} h \left(\frac{dwi}{dr} + \psi i_1 \right) \tag{22}$$

$$Yi_r^L = \frac{3}{80} G_{rz} \psi i_2 h^5 + \frac{1}{12} G_{rz} h^3 \left(\frac{dwi}{dr} + \psi i_1 \right) \tag{23}$$

$$Mi_r^L = \frac{h^5}{80\left(1-\nu_{r\theta}\nu_{\theta r}\right)} \left(E_r \frac{d\psi i_2}{dr} + \frac{\nu_{r\theta} E_\theta}{r} \psi i_2 \right) + \frac{h^3}{12\left(1-\nu_{r\theta}\nu_{\theta r}\right)} \left(E_r \frac{d\psi i_1}{dr} + \frac{\nu_{r\theta} E_\theta}{r} \psi i_1 \right) \tag{24}$$

$$Mi_\theta^L = \frac{h^5}{80\left(1-\nu_{r\theta}\nu_{\theta r}\right)} \left(\nu_{r\theta} E_\theta \frac{d\psi i_2}{dr} + \frac{E_\theta}{r} \psi i_2 \right) + \frac{h^3}{12\left(1-\nu_{r\theta}\nu_{\theta r}\right)} \left(\nu_{r\theta} E_\theta \frac{d\psi i_1}{dr} + \frac{E_\theta}{r} \psi i_1 \right) \tag{25}$$

$$Hi_r^L = \frac{h^7}{448\left(1-\nu_{r\theta}\nu_{\theta r}\right)} \left(E_r \frac{d\psi i_2}{dr} + \frac{\nu_{r\theta} E_\theta}{r} \psi i_2 \right) + \frac{h^5}{80\left(1-\nu_{r\theta}\nu_{\theta r}\right)} \left(E_r \frac{d\psi i_1}{dr} + \frac{\nu_{r\theta} E_\theta}{r} \psi i_1 \right) \tag{26}$$

$$Hi_\theta^L = \frac{h^7}{448\left(1-\nu_{r\theta}\nu_{\theta r}\right)} \left(\nu_{r\theta} E_\theta \frac{d\psi i_2}{dr} + \frac{E_\theta}{r} \psi i_2 \right) + \frac{h^5}{80\left(1-\nu_{r\theta}\nu_{\theta r}\right)} \left(\nu_{r\theta} E_\theta \frac{d\psi i_1}{dr} + \frac{E_\theta}{r} \psi i_1 \right) \tag{27}$$

In this study, the governing equations and also the boundary conditions are derived based on the principle of minimum total potential energy respectively. The basic relations are presented as follow:

$$\delta \prod i = \delta U i + \delta \Omega i = 0 \tag{28}$$

$$\delta U i = \iiint_v \left(\sigma i_r^{NL} \delta \varepsilon i_r + \sigma i_\theta^{NL} \delta \varepsilon i_\theta + \sigma i_{rz}^{NL} \delta \gamma i_{rz} \right) dV \tag{29}$$

$$\delta \Omega 1 = \int_{r_i}^{r_o} \int_0^{2\pi} \left(k_o \left(w_2 - w_1 \right) \right) \delta w r dr d\theta \quad \textit{Upper layer} \tag{30}$$

$$\delta \Omega i = \int_{r_i}^{r_o} \int_0^{2\pi} \left(-k_o \left(w_i - w_{i-1} \right) + k_o \left(w_{i+1} - w_i \right) \right) \delta w r dr d\theta \qquad \left(i = 2 ... n-1 \right) \tag{31}$$

Second layer down to the layer before the bottom layer

$$\delta \Omega n = \int_{r_i}^{r_o} \int_0^{2\pi} \left(-k_o \left(w_n - w_{n-1} \right) - k_w w_n + k_p \nabla^2 w_n \right) \delta w r dr d\theta \quad \textit{Bottom layer} \tag{32}$$

$$\delta \Omega_T = \int_0^{2\pi} \int_{r_i}^{r_o} N_r^T \left(\delta u i \right) dr d\theta \tag{33}$$

U and Ω are the internal strain energy and potential of external applied forces, respectively. N_r^T is radial in-plane load. By using the variation principals, the governing equations of multi-layer annular/circular graphene sheets are obtained in Cylindrical coordinates system in terms of local force, moment and the shear force resultants by substituting Eqs. (16-18) into the non-local form of the governing equations as follows:

$$\delta u i : N i_{r,r}^L + \frac{1}{r} \left(N i_r^L - N i_\theta^L + N_r^T \right) = 0 \tag{34}$$

$$\delta w_1 : Q1^L_{r,r} + \frac{1}{r} Q1^L_r + \left(1 - \mu\nabla^2\right)\left(k_o\left(w_2 - w_1\right) + N1^L_r \frac{1}{r}\frac{dw_1}{dr} + N1^L_{r,r}\frac{dw_1}{dr} + N1^L_r \frac{d^2 w_1}{dr^2}\right) = 0 \;\; \textit{Upper layer} \tag{35}$$

$$\delta w_i : Qi^L_{r,r} + \frac{1}{r} Qi^L_r + \left(1 - \mu\nabla^2\right)\left(-k_o\left(w_i - w_{i-1}\right) + k_o\left(w_{i+1} - w_i\right) + Ni^L_r \frac{1}{r}\frac{dw_1}{dr} + Ni^L_{r,r}\frac{dw_i}{dr} + Ni^L_r \frac{d^2 w_i}{dr^2}\right) = 0 \quad i = 2...n-1 \tag{36}$$

$$\delta w_n : Qn^L_{r,r} + \frac{1}{r} Qn^L_r + \left(1 - \mu\nabla^2\right)\left(k_p\nabla^2 w_n - k_w w_n - k_o\left(w_n - w_{n-1}\right) + Nn^L_r \frac{1}{r}\frac{dw_n}{dr} + Nn^L_{r,r}\frac{dw_n}{dr} + Nn^L_r \frac{d^2 w_n}{dr^2}\right) = 0 \;\; \textit{Bottom layer} \tag{37}$$

$$\delta\psi i_1 : Mi^L_{r,r} + \frac{1}{r}\left(Mi^L_r - Mi^L_\theta\right) - Qi^L_r = 0 \tag{38}$$

$$\delta\psi i_2 : Hi^L_{r,r} + \frac{1}{r}\left(Hi^L_r - Hi^L_\theta\right) - 3Yi^L_r = 0 \tag{39}$$

2.1.1 The adjacent equilibrium estate method

In this paper, the adjacent equilibrium estate method is applied to calculate the critical temperature leading to unstable statement. The equilibrium equation can be obtained from the very small variations near equilibrium estate. Consequently, the displacement, force and moment resultants are defined as follows:

$$ui = ui^0 + ui^1, wi = wi^0 + wi^1, \psi i_1 = \psi i_1{}^0 + \psi i_1{}^1, \psi i_2 = \psi i_2{}^0 + \psi i_2{}^1$$
$$Ni_r = Ni_r^0 + Ni_r^1, Ni_\theta = Ni_\theta^0 + Ni_\theta^1$$
$$Qi_r = Qi_r^0 + Qi_r^1$$
$$Mi_r = Mi_r^0 + Mi_r^1, Mi_\theta = Mi_\theta^0 + Mi_\theta^1, Hi_r = Hi_r^0 + Hi_r^1, Hi_\theta = Hi_\theta^0 + Hi_\theta^1$$

The superscript (0) sets for the pre-buckling state and superscript (1) for very small changes in buckling state. Since there is not any deflection in pre-buckling conditions, so, $wi^0, \psi i_1{}^0, \psi i_2{}^0 = 0$. By solving pre-buckling equations it can be concluded:

$$N_r^0 = N_\theta^0 = N_r^T = \frac{E_r\alpha\left(1+\nu_{r\theta}\right)\cdot\Delta T}{1-\nu_{r\theta}\nu_{\theta r}}h$$

By using the mentioned definitions, the buckling governing equations for multi-layer annular/circular graphene sheets are obtained below:

$$\delta ui^1 : Ni^{1L}_{r,r} + \frac{1}{r}\left(Ni^{1L}_r - Ni^{1L}_\theta\right) = 0 \tag{40}$$

$$\delta w_1^1 : Q1^{1L}_{r,r} + \frac{1}{r} Q1^{1L}_r + \left(1 - \mu\nabla^2\right)\left(k_o\left(w_2^1 - w_1^1\right) + \left(N1^{1L}_r + N1^{0L}_r\right)\frac{1}{r}\frac{dw_1^1}{dr} + \left(N1^{1L}_{r,r} + N1^{0L}_{r,r}\right)\frac{dw_1^1}{dr} + \left(N1^{1L}_r + N1^{0L}_r\right)\frac{d^2 w_1^1}{dr^2}\right) = 0 \;\; \textit{Upper layer} \tag{41}$$

$$\delta w_i^1 : Qi_{r,r}^{1L} + \frac{1}{r} Qi_r^{1L} + \left(1 - \mu\nabla^2\right)\left(-k_o\left(w_i^1 - w_{i-1}^1\right) + k_o\left(w_{i+1}^1 - w_i^1\right) + \left(Ni_r^{1L} + Ni_r^{0L}\right)\frac{1}{r}\frac{dw_i^1}{dr} \right.$$
$$\left. + \left(Ni_{r,r}^{1L} + Ni_{r,r}^{0L}\right)\frac{dw_i^1}{dr} + \left(Ni_r^{1L} + Ni_r^{0L}\right)\frac{d^2 w_i^1}{dr^2} \right) = 0 \qquad i = 2...n-1 \tag{42}$$

$$\delta w_n^1 : Qn_{r,r}^{1L} + \frac{1}{r} Qn_r^{1L} + \left(1 - \mu\nabla^2\right)\left(k_p \nabla^2 w_n^1 - k_w w_n^1 - k_o\left(w_n^1 - w_{n-1}^1\right) + \right.$$
$$\left. \left(Nn_r^{1L} + Nn_r^{0L}\right)\frac{1}{r}\frac{dw_n^1}{dr} + \left(Nn_{r,r}^{1L} + Nn_{r,r}^{0L}\right)\frac{dw_n^1}{dr} + \left(Nn_r^{1L} + Nn_r^{0L}\right)\frac{d^2 w_n^1}{dr^2} \right) = 0 \quad Bottom\ layer \tag{43}$$

$$\delta\psi i_1^1 : Mi_{r,r}^{1L} + \frac{1}{r}\left(Mi_r^{1L} - Mi_\theta^{1L}\right) - Qi_r^{1L} = 0 \tag{44}$$

$$\delta\psi i_2^1 : Hi_{r,r}^{1L} + \frac{1}{r}\left(Hi_r^{1L} - Hi_\theta^{1L}\right) - 3Yi_r^{1L} = 0 \tag{45}$$

Since, the numbers are extremely small in nano scales, due to convenience and avoiding the digits error in processing, the non-dimensional terms are introduced as follow. After substituting these terms into the resultant components and then into the governing equations (Eqs. (40-45)), the dimensionless form of equations would be obtained in terms of displacements and rotations.

$$r^* = \frac{r}{r_o}; ui^* = \frac{ui}{h}; wi^* = \frac{wi}{r_o}; z^* = \frac{z}{h}; \psi i_1^* = \psi i_1; \psi_2^* = \frac{\psi_2}{h^2}; \eta = \frac{h}{r_o};\ \mu^* = \frac{\mu}{r_o^2};\ q^* = \frac{q}{E_r};\ k_w^* = \frac{k_w r_o}{E_r}; k_p^* = \frac{k_p}{E_r h}$$
$$\rho 1 = \frac{E_\theta}{E_r}; \rho 2 = \frac{G_{rz}}{E_r}; \upsilon = 1 - v_{r\theta} v_{\theta r}$$

2.1.2 Boundary conditions

The boundary conditions are derived from Eqs. (28-33) in the category of the simply supported (S), clamped (C) and free edges (F). The definition for the boundary conditions is shown in Fig. 3.

$$S : ui = wi = Mi_r = Hi_r = 0 \qquad r = r_i, r_o$$
$$C : ui = wi = \psi i_1 = \psi i_2 = 0 \qquad r = r_i, r_o$$
$$F : Ni_r = Qi_r = Mi_r = Hi_r = 0 \qquad r = r_i, r_o$$

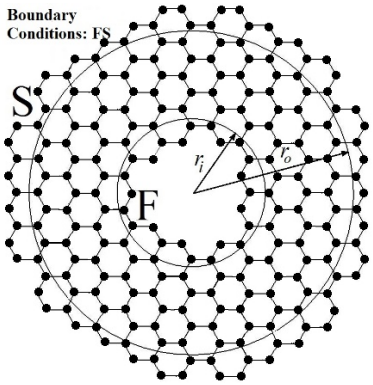

Fig.3
Definition of the boundary conditions.

2.2 FSDT formulation

The FSDT displacement field can be expressed by neglecting z^3 in Eq. (1) as follow:

$$Ui(r,z)=ui(r)+z\psi i_1(r) \tag{46}$$

$$Vi(r,z)=0 \tag{47}$$

$$Wi(r,z)=wi(r) \tag{48}$$

The procedure which is explained for TSDT analysis, is repeated to obtain the governing equations for FSDT analysis. The governing equations can be expressed as follow:

$$\delta ui: Ni^L_{r,r}+\frac{1}{r}\left(Ni^L_r-Ni^L_\theta\right)=0 \tag{49}$$

$$\delta w_1: Q1^L_{r,r}+\frac{1}{r}Q1^L_r+\left(1-\mu\nabla^2\right)\left(k_o\left(w_2-w_1\right)+N1^L_r\frac{1}{r}\frac{dw_1}{dr}+N1^L_{r,r}\frac{dw_1}{dr}+N1^L_r\frac{d^2w_1}{dr^2}\right)=0 \ \textit{Upper layer} \tag{50}$$

$$\delta w_i: Qi^L_{r,r}+\frac{1}{r}Qi^L_r+\left(1-\mu\nabla^2\right)\left(-k_o\left(w_i-w_{i-1}\right)+k_o\left(w_{i+1}-w_i\right)+Ni^L_r\frac{1}{r}\frac{dw_1}{dr}+Ni^L_{r,r}\frac{dw_i}{dr}+Ni^L_r\frac{d^2w_i}{dr^2}\right)=0 \tag{51}$$

$i=2...n-1$

$$\delta w_n: Qn^L_{r,r}+\frac{1}{r}Qn^L_r+\left(1-\mu\nabla^2\right)\left(k_p\nabla^2w_n-k_ww_n-k_o\left(w_n-w_{n-1}\right)+Nn^L_r\frac{1}{r}\frac{dw_n}{dr}+Nn^L_{r,r}\frac{dw_n}{dr}+Nn^L_r\frac{d^2w_n}{dr^2}\right)=0 \tag{52}$$

Bottom layer

$$\delta\psi i_1: Mi^L_{r,r}+\frac{1}{r}\left(Mi^L_r-Mi^L_\theta\right)-Qi^L_r=0 \tag{53}$$

The stress resultants are obtained as follow:

$$Ni^L_r=\frac{E_rh}{1-\nu_{r\theta}\nu_{\theta r}}\left(\frac{dui}{dr}+\frac{1}{2}\left(\frac{dwi}{dr}\right)^2-\alpha\cdot\Delta T\right)+\frac{\nu_{r\theta}E_\theta h}{1-\nu_{r\theta}\nu_{\theta r}}\left(\frac{ui}{r}-\alpha\cdot\Delta T\right) \tag{54}$$

$$Ni^L_\theta=\frac{\nu_{r\theta}E_\theta h}{1-\nu_{r\theta}\nu_{\theta r}}\left(\frac{dui}{dr}+\frac{1}{2}\left(\frac{dwi}{dr}\right)^2-\alpha\cdot\Delta T\right)+\frac{E_\theta h}{1-\nu_{r\theta}\nu_{\theta r}}\left(\frac{ui}{r}-\alpha\cdot\Delta T\right) \tag{55}$$

$$Qi^L_r=\frac{1}{4}\kappa_sG_{rz}\psi i_2h^3+\kappa_sG_{rz}h\left(\frac{dwi}{dr}+\psi i_1\right) \tag{56}$$

$$Mi^L_r=\frac{h^3}{12\left(1-\nu_{r\theta}\nu_{\theta r}\right)}\left(E_r\frac{d\psi i_1}{dr}+\frac{\nu_{r\theta}E_\theta}{r}\psi i_1\right) \tag{57}$$

$$Mi^L_\theta=\frac{h^3}{12\left(1-\nu_{r\theta}\nu_{\theta r}\right)}\left(\nu_{r\theta}E_\theta\frac{d\psi i_1}{dr}+\frac{E_\theta}{r}\psi i_1\right) \tag{58}$$

k_s is the transverse shear correction coefficient which is taken 5/6 [18]. By the same mentioned explanations for TSDT analysis in section 2.1, the stability governing equations can be derived for FSDT analysis, again.

2.2.1 Boundary conditions (FSDT)

In this paper, the boundary conditions are assumed the simply supported (S), clamped (C) and free edges (F) like TSDT analysis, the boundary conditions are given for each boundaries as follow:

$$S: ui = wi = Mi_r = 0 \qquad r = r_i, r_o$$
$$C: ui = wi = \psi i_1 = 0 \qquad r = r_i, r_o$$
$$F: Ni_r = Qi_r = Mi_r = 0 \qquad r = r_i, r_o$$

3 SOLUTION (DIFFERENTIAL QUADRATURE METHOD (DQM))

In this study, the differential quadrature method (DQM) is used to solve the equilibrium equations for different types of boundary conditions. The DQM was proposed by Bellman and coworkers for solving differential equations [27, 28]. This method is highly accurate, convenient and capable to solve the partial differential equations, so, many researchers have used the DQM to analyze the sets of ordinary and partial differential equations system. In this method, the derivatives of a function at any grid points is approximated using weighted sum of all the functional values at certain points in the whole computational domain.

By using the DQ Method, derivatives of a function $f(r)$ at point r can be defined as following linear sum of the function values:

$$\left.\frac{d^{(n)}f}{dr^{(n)}}\right|_{r_i} = \sum_{j=1}^{N} A_{ij}^{(n)} f(r_i) \quad i = 1, ..., N \tag{59}$$

$$A_{ij}^{(n)} = n\left[A_{ij}^{(1)} A_{ii}^{(n-1)} - \frac{A_{ij}^{(n-1)}}{\left(r_i - r_j\right)}\right] \quad i \neq j, A_{ii}^{(n)} = -\sum_{j=1,\neq i}^{N} A_{ij}^{(n)} \quad i, j = 1...N \tag{60}$$

In which, N is the number of grid points along r direction. It is more offered to use the grid point distribution which is based on Gauss-Chebyshev-Lobatto points to gain more accurate results [18].

By use of DQM, the set of differential equations is transformed to the non-linear algebraic equations system instead of non-linear ordinary differential equations system.

4 NUMERICAL RESULTS AND DISCUSSION

First, it is considered a single layer annular graphene sheet to check the convergence of DQM for TSDT analysis. Fig. 4 shows that the converged results are obtained by only nine nodes along the r direction for different types of boundary conditions. There is not any difference in the rate of convergence for different types of boundary conditions.

$$E_r = 1.06\times10^{12}\ \text{Pa}; E_\theta = 0.85\times10^{12}\ \text{Pa};\ \nu_{r\theta}=\nu_{\theta r}=0.3; r_i / r_0 = 0.2;\ h = 0.34nm; \alpha = 2.02\times10^{-6}$$

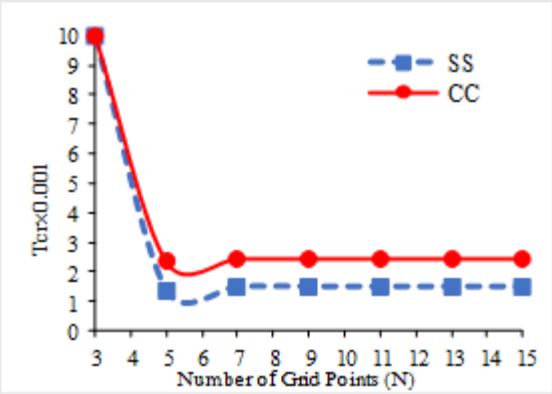

Fig. 4
Variation of critical temperature versus the number of nodes for DQM domain.

Table 1. shows the comparison between the obtained results of this paper and the other references for different values of the thickness and r_i / r_o ratio. The results of this paper are inconsiderably less than the Ref [29, 30] because of applying TSDT analysis. However, the accuracy and agreement of the results can be observed. Consequently, applying TSDT analysis and DQM method gives appropriate and accurate results.

Table 1
Comparison of critical temperature with the other references for circular plate.

h/r_o	$r_i/r_o=0.2$			$r_i/r_o=0.4$			$r_i/r_o=0.6$		
	[29]	[30]	Present paper	[29]	[30]	Present paper	[29]	[30]	Present paper
SS									
0.05	18.5471	18.5471	18.3059	28.6417	28.6332	28.3266	60.1986	60.1865	59.77721
0.1	17.7252	17.7241	17.4947	26.9211	26.9153	26.6249	53.2518	53.2462	52.87903
0.15	16.5100	16.5079	16.2953	24.4721	24.4629	24.2029	44.6630	44.6624	44.35035
0.2	15.0695	15.0699	14.8735	21.7093	21.7062	21.4704	36.4367	36.4332	36.18164
SC									
0.05	40.7178	40.1322	40.1884	61.1677	61.1680	60.4948	122.3041	122.1025	121.4479
0.1	37.4454	36.7599	36.9586	53.9609	53.9490	53.3673	95.9334	95.9224	95.26186
0.15	33.0228	32.2851	32.5935	45.1082	45.1046	44.6120	70.6129	70.5936	70.11861
0.2	28.3376	27.6045	27.9692	36.6890	36.5904	36.2854	51.6063	51.5236	51.24505
CS									
0.05	27.9670	27.8256	27.6034	49.9565	49.9566	49.4069	109.5716	109.4116	108.8046
0.1	25.9118	25.6137	25.5749	44.2265	44.2225	43.7400	86.1880	86.1740	85.58468
0.15	23.0852	22.7338	22.7850	37.1368	37.1246	36.7282	63.6357	63.6325	63.19025
0.2	20.0331	19.7580	19.7726	30.3496	30.3490	30.0157	46.6745	46.6625	46.34777

As it is mentioned before, in this study in addition to TSDT, the FSDT analysis is considered too. Comparison between the FSDT and TSDT analyses is shown in Table 2. by considering a single layer annular graphene sheet with clamped-clamped (CC) edges with the conditions below:

$$E_r = 1.06\times10^{12}\ \text{Pa}; E_\theta = 0.85\times10^{12}\ \text{Pa};\ \nu_{r\theta}=\nu_{\theta r}=0.3; r_i / r_0 = 0.2;\ h = 0.34nm; \alpha = 2.02\times10^{-6}$$

According to Table 2. , it is concluded that the buckling temperature decreases with the increase of non-local parameter for both FSDT and TSDT analyses. TSDT analysis gives the smaller results in comparison with FSDT in this problem. However, it is observed that two theories distance with increase of the small scale effects. Consequently, it can be possible to use FSDT analysis instead of TSDT for smaller values of non-local parameters which is caused inconsiderable differences between the obtained results of two theories.

The comparison between TSDT and FSDT analyses is illustrated for different types of boundary conditions and thicknesses in Table 3. The critical temperature increases with increase of thickness. The rate of increasing of the critical temperature for FSDT analysis is more than TSDT. It is also seen that the difference between two theories

are more significant for the higher values of thickness. For example, there is about 5 percent difference between the results of FSDT and TSDT analyses for $h^* = 4$. Applying TSDT analysis gives more accurate results in comparison with FSDT in any circumstances. Also, the differences between FSDT and TSDT analyses for CC boundary conditions is more than SS along the rise of h^*.($h^* = h/(0.34nm)$).

Table 2
Comparison between TSDT and FSDT analysis for different non-local parameter.

$e_0a(nm)$	$\Delta T_{cr}(C^\circ)$		R_t = TSDT/FSDT
	FSDT	TSDT	
0	8341.03	8341.02	1
0.5	5166.23	5165.86	0.999928381
1	2430.93	2420.20	0.995586051
1.5	1222.85	1068.96	0.874154639
2	719.07	607.57	0.844938601

Table 3
Comparison between TSDT and FSDT analyses for different types of boundary conditions and thicknesses ($\mu = 1nm^2$).

	$\Delta T_{cr}(C^\circ)$			
	h^*	TSDT	FSDT	R_t = TSDT/FSDT
CC	1	2420.20	2430.93	0.995586051
	2	7749.75	7867.30	0.985058406
	3	13405.23	13813.65	0.970433593
	4	18339.55	19118.09	0.959277313
SS	1	1507.63	1509.41	0.998820731
	2	5581.47	5587.84	0.998860025
	3	11244.72	11335.07	0.992029163
	4	18438.17	18124.95	0.983012333

4.1 Sample 1: Single layer annular graphene sheet

A single layer annular/circular graphene sheet is assumed with the material properties below. The variation of critical temperature versus the non-local parameter is demonstrated in Fig.5 in different types of boundary conditions. The buckling temperature decreases along the increase of small scale effects for all types of boundary conditions. If the non-local parameter is considered to be zero, the critical temperature for CC boundary conditions is more than the other boundaries. It is concluded that whatever the boundary conditions is more flexible, the buckling load is smaller. SS and FS results are closer in comparison with CC and FC. However, the buckling temperature for all boundary conditions approach with growing the non-local parameter.

$$E_r = 1.06\times10^{12}\,\text{Pa}; E_\theta = 0.85\times10^{12}\,\text{Pa};\ \nu_{r\theta}=\nu_{\theta r}=0.3; r_i/r_0 = 0.2;\ h = 0.34nm; k_w = 1.13Gpa/nm;$$
$$k_p = 1.13Pa.m; \alpha = 2.02\times10^{-6}$$

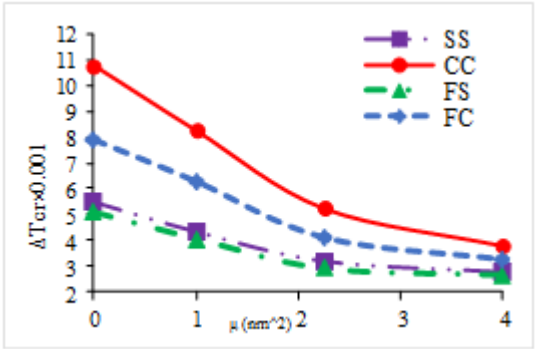

Fig. 5
Variation of critical temperature versus the non-local parameter for different types of boundary conditions.

Fig. 6 is drawn to study the effect of plate's size on the results. The thickness is a constant value and the outer radius r_o varies in r_o / h ratio. It is observed that ΔT_{cr} increases and tends to a constant value during the increase of r_o / h. The buckling temperature decreases for the bigger value of non-local parameter (conclusion in Fig. 4). The rate of convergence of ΔT_{cr} to a constant value for smaller values of non-local parameter, is more than the larger ones. It is also seen that for the same non-local parameter and the large enough value of r_o / h the results of CC and SS boundary conditions are so close to each other.

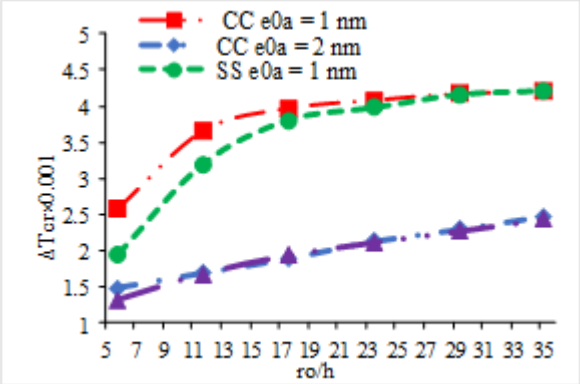

Fig. 6
Variation of the critical temperature versus the r_o / h ratio.

The parameter T_m is defined as $T_m = \Delta T_{cr}^{Nonlocal} / \Delta T_{cr}^{Local}$ to study the effect of non-local investigation on the results. Fig. 7 describes the effect of non-local analysis. For small sizes of the plate (small values of r_o / h ratio), the local and non-local analyses are distanced too far. On the other hand, the small scales effects increases remarkably in small sizes and the importance of applying the non-local analysis increases. Then, the small scale effects decrease along the rise of r_o / h and the local and non-local analyses approach. Also, the effect of applying the non-local analysis for CC boundary conditions is more than SS as it is observed the local and non-local analyses are closer for SS boundary conditions. It can be concluded that the small scale effects is lesser for more flexible boundary conditions.

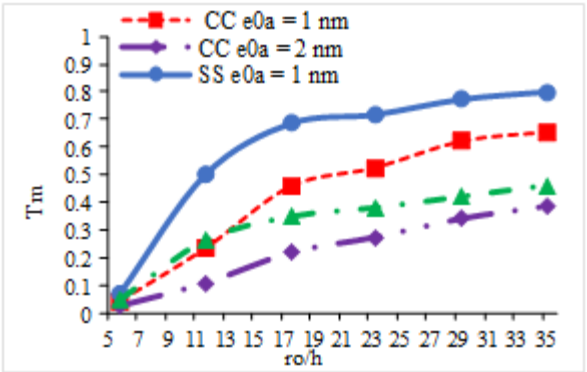

Fig. 7
Variation of T_m parameter versus the r_o / h ratio.

The effect of Winkler and Pasternak elastic foundations is investigated for CC boundary conditions, Fig. 8 (a) the Winkler and (b) the Pasternak elastic matrixes. The variations are linear for both Winkler and Pasternak foundations. According to Fig. 8 (a) and (b), the buckling temperature increases along the increase of the Winkler and Pasternak elastic foundations. However, the effect of Pasternak elastic foundation is more significant on the results as it is observed its slope is steeper in comparison with the Winkler foundation. In addition, ΔT_{cr} is distanced more for the Winkler foundation in comparison with the Pasternak foundation along the rise of small scale effects.

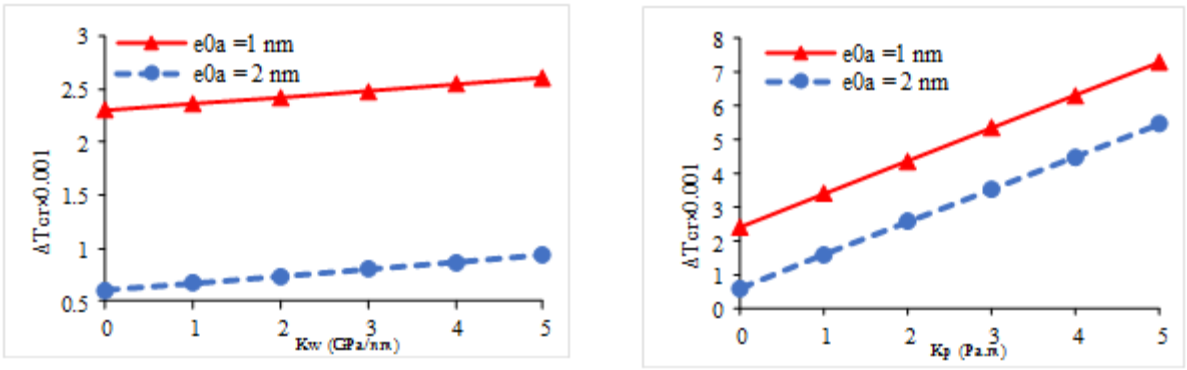

(a) (b)

Fig. 8
Variation of ΔT_{cr} versus (a) the Winkler and (b) the Pasternak elastic foundations.

4.2 Sample 2: Bilayer annular graphene sheet

A bi-layer graphene sheet is considered. The variations of buckling temperature versus the van der Waals interaction between the layers are shown in Fig. 9 (a) for CC and (b) for SS boundary conditions. ΔT_{cr} grows and tends to a constant value with increase of the van der Waals interaction between two layers for both boundary conditions and the value of non-local parameter. The variations are more considerable for smaller value of the non-local parameters. On the other hand, whatever the non-local parameter rises the critical temperature enlarges gently, whereas the curve slope is steeper for small values of the non-local parameters.

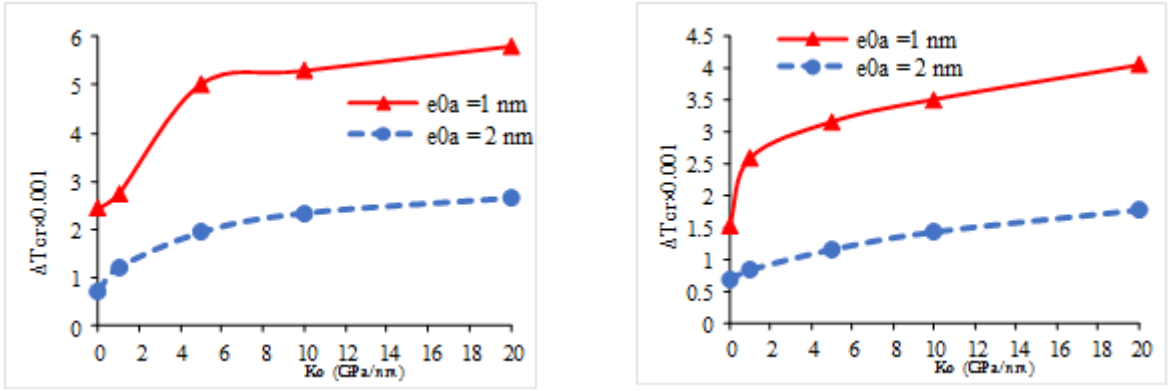

(a) (b)

Fig. 9
Variations of ΔT_{cr} versus the van der Waals interaction between two layers (a) CC (b) SS boundary conditions.

4.3 Sample 3: Triple and multi-layer plate

The previous graphs that are pictured for bi-layer sheets are repeated for triple layers. The results are illustrated in Fig. 10 all the mentioned conclusions which are explained for bi-layer plate are true for triple layers. However, according to Fig. 10 (a,b) there is slight difference between the results of CC and SS boundary conditions, whereas it is obvious for bi-layer sheets. It can be concluded that whatever the number of layers increases, the effect of boundary conditions would be decreased on the results. Also, as it was expected, the critical temperature for triple layer sheet is more than the same bi-layer plate by comparing Figs. 9 and 10. The procedure for calculating the critical temperature for multi-layer sheets is the same as bi-layer and triple layer sheets. However, whatever the

number of the layers increases, the computational process increases. In addition, it can be possible to calculate the differences between the results of bi-layer and single layer, triple layer and bi-layer sheets, afterwards, generalize it to predict a logical procedure for the results of multi-layer sheets.

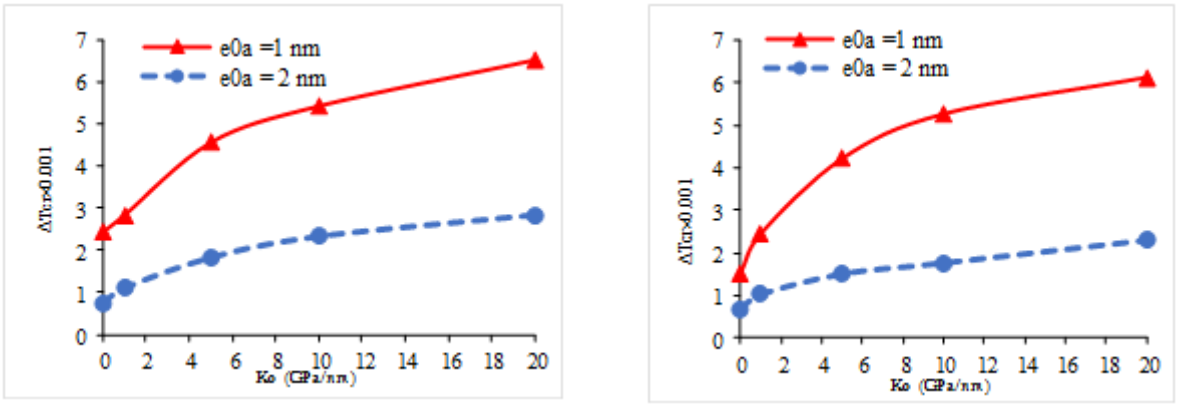

(a) (b)

Fig. 10
Variations of ΔT_{cr} versus the van der Waals interaction between three layers (a) CC (b) SS boundary conditions.

5 CONCLUSIONS

In this article, the solution for thermo-elastic buckling of multi-layer graphene sheets is investigated based on FSDT and TSDT non-local theory of Eringen. The generalized stability equations are obtained in terms of displacements and rotations considering the van der Waals interaction between the layers. The DQM, which is an accurate numerical method, is applied to solve the governing equations. Different types of boundary conditions including clamped, simply supported and free edges are considered. The critical temperature is obtained for various types of boundary conditions, the non-local parameters, the non-local to local analyses and FSDT to TSDT analyses. The buckling temperature is calculated for bi-layer and triple layer sheets. The main conclusions of this paper can be summarized as follow:

- The TSDT analysis gives the more accurate results in comparison with the FSDT analysis especially for high values of thickness.
- The results of FSDT and TSDT analyses distance with increase of non-local parameter.
- The buckling temperature decreases with increase of the small scale effect.
- Whatever the plate is more flexible, the effects of non-local parameter decreases.
- With increase of the plate's size, the local and non-local analyses approach.
- The effect of Pasternak elastic foundation on the buckling temperature is more significant than the Winkler.
- The critical temperature increases and tends to a constant value along the increase of the van der Waals interaction between the layers for bi-layer and triple layer graphene sheets.
- Whatever the number of the layers increases, the effect of boundary conditions decreases on the results.

REFERENCES

[1] Boehm H.P., Setton R., Stumpp E., 1994, Nomenclature and terminology of graphite intercalation compounds, *Pure and Applied Chemistry* **66**: 1893-1901.

[2] Novoselov K.S., Geim A.K., Morozov S.V., Jiang D., Zhang Y., Dubonos S.V., Grigorieva I.V., Firsov A.A., 2004, Electric field effect in atomically thin carbon films, *Science* **306**: 666-669.

[3] Reddy J.N., 2011, Microstructure-dependent couple stress theories of functionally graded beams, *Journal of the Mechanics and Physics of Solids* **59**(11): 2382-2399.

[4] Akgöz B., Civalek Ö., 2013, A size-dependent shear deformation beam model based on the strain gradient elasticity theory, *International Journal of Engineering Science* **70**: 1-14.

[5] Akgöz B., Civalek Ö., 2013, Buckling analysis of functionally graded micro beams based on the strain gradient theory, *Acta Mechanica* **224**: 2185-2201.
[6] Lam D.C.C., Yang F., Chong A.C.M., Wang J., Tong P., 2003, Experiments and theory in strain gradient elasticity, *Journal of the Mechanics and Physics of Solids* **51**(8): 1477-1508.
[7] Ke L.L., Yang J., Kitipornchai S., 2011, Free vibration of size dependent Mindlin micro plates based on the modified couple stress theory, *Journal of Sound and Vibration* **331**: 94-106.
[8] Akgöz B., Civalek Ö., 2011, Strain gradient elasticity and modified couple stress models for buckling analysis of axially loaded micro scaled beams, *International Journal of Engineering Science* **49**: 1268-1280.
[9] Akgöz B., Civalek Ö., 2013, Free vibration analysis of axially functionally graded tapered Bernoulli-Euler microbeams based on the modified couple stress theory, *Composite Structures* **98**: 314-322.
[10] Yang F., Chong A.C.M., Lam D.C.C., Tong P., 2002, Couple stress based strain gradient theory for elasticity, *International Journal of Solids and Structures* **39**: 2731-2743.
[11] Eringen A.C., Edelen D.G.B., 1972, On non-local elasticity, *International Journal of Engineering Science* **10**: 233-248.
[12] Eringen A.C., 1983, On differential equations of non-local elasticity, solutions of screw dislocation, surface waves, *Journal of Applied Physics* **54**: 4703-4710.
[13] Eringen A.C., 2002, *Non-Local Continuum Field Theories*, Springer-Verlag, New York.
[14] Eringen A.C., 2006, Non-local continuum mechanics based on distributions, *International Journal of Engineering Science* **44**: 141-147.
[15] Wen C.C., Chang T.W., Kuo W.S., 2014, Experimental study on mechanism of buckling and Kink-band formation in graphene nanosheets, *Applied Mechanics & Materials* **710**: 19-24.
[16] Ghorbanpour Arani A., Kolahchi R., Allahyari S.M.R., 2014, Non-local DQM for large amplitude vibration of annular boron nitride sheets on non-linear elastic medium, *Journal of Solid Mechanics* **6**(4): 334-346.
[17] Mohammadi M., Goodarzi M., Ghayour M., AlivandS., 2012, Small scale effect on the vibration of orthotropic plates embedded in an elastic medium and under biaxial in-plane pre-load via non-local elasticity theory, *Journal of Solid Mechanics* **4**(2): 128-143.
[18] Dastjerdi S., Jabbarzadeh M., Tahani M., Nonlinear bending analysis of sector graphene sheet embedded in elastic matrix based on nonlocal continuum mechanics, *IJE Transaction B: Applications* **28**: 802-811.
[19] Anjomshoa A., Shahidi A.R., Shahidi S.H., Nahvi H., 2014, Frequency analysis of embedded orthotropic circular and elliptical micro/nano-plates using non-local variational principle, *Journal of Solid Mechanics* **7**(1): 13-27.
[20] Pradhan S.C., 2009, Buckling of single layer graphene sheet based on nonlocal elasticity and higher order shear deformation theory, *Physics letters A* **373**: 4182-4188.
[21] He X.Q., Kitipornchai S., Liew K.M., 2005, Buckling analysis of multi-walled carbon nanotubes: a continuum model accounting for van der Waals interaction, *Journal of the Mechanics and Physics of Solids* **53**: 303-326.
[22] Scarpa F., Adhikari S., Gil A.J., Remillat C., 2010, The bending of single layer graphene sheets: The lattice versus continuum approach, *Nanotechnology* **21**(12): 125702.
[23] Samaei A.T., Abbasian S., Mirsayar M.M., 2011, Buckling analysis of a single layer graphene sheet embedded in an elastic medium based on nonlocal Mindlin plate theory, *Mechanics Research Communications* **38**: 481-485.
[24] Zenkour A.M., Sobhy M., 2013, Nonlocal elasticity theory for thermal buckling of nanoplates lying on Winkler–Pasternak elastic substrate medium, *Physica E* **53**: 251-259.
[25] Wang Y., Cui H.T., Li F.M., Kishimoto K., 2013, Thermal buckling of a nanoplate with small-scale effects, *Acta Mechanica* **224**(6): 1299-1307.
[26] Pradhan S.C., Phadikar J.K., 2009, Small scale effect on vibration of embedded multilayered graphene sheets based on nonlocal continuum models, *Physics Letters A* **373**: 1062-1069.
[27] Bellman R.E., Casti J., 1971, Differential quadrature and long-term integration, *Journal of Mathematical Analysis & Applications* **34**: 235-238.
[28] Bellman R.E., Kashef B.G., Casti J., 1972, Differential quadrature: A technique for the rapid solution of nonlinear partial differential equation, *Journal of Computational Physics* **10**: 40-52.
[29] Sepahi O., Forouzan M.R., Malekzadeh P., 2011, Thermal buckling and postbuckling analysis of functionally graded annular plates with temperature-dependent material properties, *Materials and Design* **32**: 4030-4041.
[30] Wang C.M., Xiang Y., Kitipornchai S., Liew K.M., 1994, Buckling solutions for Mindlin plates of various shapes, *Engineering Structures* **16**: 119-127.